

One degree of freedom in a Random Energy Landscape

Domain wall motion in a random energy landscape

Introduction

Many features of hysteresis can be understood using the model of motion of the system state in a random energy landscape. We already saw in the introduction that the phenomenon of branching arises from this model. We also saw that the resulting hysteresis loop shape is dependent on the overall statistical properties of the free energy. The purpose of our work is to start from a random energy landscape (or, better, its derivative: the pinning field) and to study the resulting hysteretic processes.

In the model here presented the system state exhibits just one degree of freedom, which can be considered to represent, for example, the position of a domain wall. Its motion will be stochastic, having to move on a random energy profile. In physical terms, this noise can be due to the presence of non magnetic impurities, defects, dislocations, in the magnetic medium in which the DW moves. We will show in this and in the next chapter that, notwithstanding the great number of initial simplifications, it is possible to obtain from this model a certain amount of information on many physical observables, like the Rayleigh parameters [Magni *et al.* 1996], the Barkhausen noise amplitude distribution and its power spectrum [Alessandro *et al.* 1990a, 1990b], its fractal dimension and the duration and size distributions of single Barkhausen jumps [Durin, Magni 1996; Durin, Bertotti, Magni 1995].

In this chapter and in the next one, we will always suppose that the system is adiabatic: the external forces driving the system state – i.e. the external field – will change infinitely slowly. This means that at any time the system will always be in a stable state, excluding the Barkhausen jumps. At the same time, we will not consider thermal relaxation, so if the system will be initially in a locally stable state, in the absence of external forces it will stay there indefinitely. Finally, many other features connected to the magnetization will be neglected, above all the dynamical effects: they will be addressed in the following chapter.

Precursors

Néel

Néel [Néel 1942, Néel 1943] introduced the concept of random energy landscape, in the framework of an explanation of the Rayleigh law on a statistical basis.

His calculations start from the displacement of a single DW, of surface S , separating two contiguous domains with magnetization \mathbf{I} and \mathbf{J} , respectively. This DW displacement generates a surface energy variation dE_p and a magnetocrystalline energy variation dE_u . The energy variations arise from the fact that the surface energy density γ and the magnetocrystalline energy densities u_i , with $i=1,2,3$ for the three coordinate axes, are function of the position of the DW. They vary in space due to the local fluctuations of the medium at low scale, while Néel excluded from his calculations the presence of large scale fluctuations.

The magnetic energy variation for a displacement dx from the equilibrium position under the external field \mathbf{H} is:

dE

$$\mathbf{H} = (\mathbf{J} - \mathbf{I}) \cdot \mathbf{H} S dx \quad [1]$$

One degree of freedom in a Random Energy Landscape

so that the pressure exerted by the external field is

$V =$

$$(\mathbf{J} - \mathbf{I}) \cdot \mathbf{H} \quad [2]$$

By introducing the stochastic function E , whose differential is $dE = dEp + dEu$, at the stable equilibrium position x we must have

$$\begin{cases} V = \frac{1}{S} \frac{dE}{dx} \\ \frac{d^2 E}{dx^2} > 0 \end{cases} \quad [3]$$

Within the hypothesis of neglecting the large scale fluctuations, the function E/S fluctuates around a constant mean value and represents the random energy profile experienced by the DW during its motion.

At this point Néel delineated his hypothesis for the energy profile. He supposed it as a sequence of parabolic arcs equispaced of $2l$. In this case, the energy gradient is a polygonal line of segments of length $2l$ and random slope. We then have just two parameters: the distance $2l$ between adjacent points of the sequence and the characteristic slope P_0 , related to the width of the gaussian distribution of the slopes of the segments describing the pinning field:

$$\omega(P) = \frac{1}{\sqrt{\pi}} e^{-\{P/P_0\}^2} \quad [4]$$

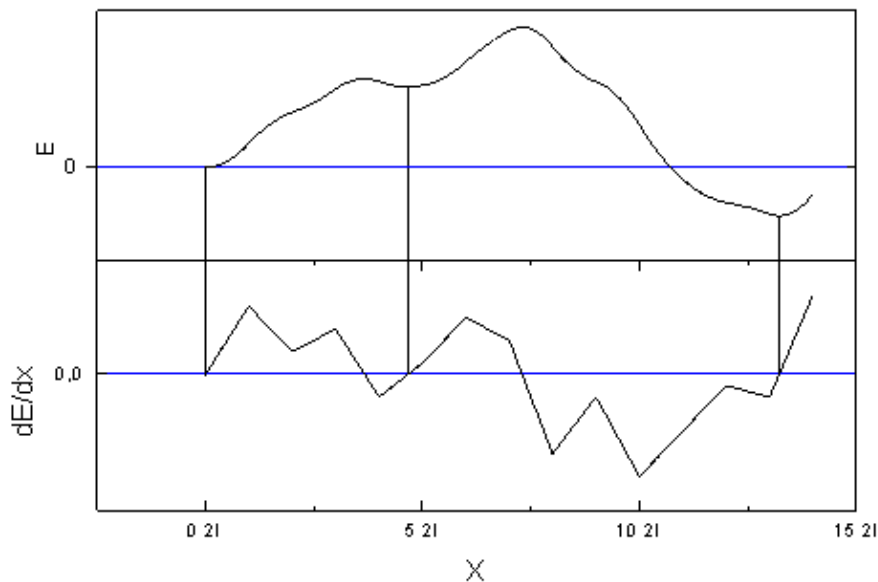


Fig.1 Néel's energy landscape, and its derivative. The x axis is in $2l$ units.

One degree of freedom in a Random Energy Landscape

A notable feature worth mentioning is that for DW displacements lower than $2l$ the DW moves in a reversible way, while higher displacements can lead to irreversible jumps. The $2l$ distance is then the threshold of the reversible motion region. Moreover, after a $2l$ step a new slope P is chosen, from the gaussian distribution [Eq.4]. Due to the fact that the choice is not influenced from the previous slope value, we can observe that $2l$ represents also the distance beyond which the memory of both the stochastic function values and their slope are erased.

Trauble, Pfeffer and Kronmuller

In the approach developed by Pfeffer, Trauble, Kronmuller *et al.*, [Pfeffer 1967, Kronmuller *et al.* 1992, Hilzinger *et al.* 1976, Reininger *et al.* 1992] one assumes that local fluctuations of the defect concentration are effective as pinning centers. The field $V(x)$ acting on the DW at position x is the superposition of different interaction forces $u(x-x_j)$ for the different defects at position x_j : $V(x) = \sum_j u(x-x_j)$, where the sum

extends over all defects. Such a description of the pinning field (we always identify by this term the derivative of the energy profile) generalizes the simple saw-tooth structure used by Néel in his model. The pinning field depends upon three parameters: average wave length $2l$; average value \bar{V}_{\max} of the maxima of $V(x)$; reciprocal of the average value of the slopes of $V(x)$ at $V(x)=0$: $1/\bar{R}$. By assuming $V(x)$ to be gaussian distributed, it has been predicted its influence on the coercive field:

$$H_c = \frac{\max_{0 < x < L_3} (V(x))}{2l, F_B} \quad [5]$$

and on the initial susceptibility:

$$\chi = \frac{4l^2 F_B}{L_3} \left\langle \left(\left(\frac{dV}{dx} \right)_{H=0}^{-1} \right) \right\rangle \quad [6]$$

From the calculation of the pinning field and slope distributions, it has been obtained that they result to be gaussian.

One notable result concerning this kind of energy landscape is the discovery that the energy average value at a given position is proportional to the local slope. This means that the deepest energy wells (more stable states) are even the steepest. From this conclusion it has been derived that the occupation probability of a given state with local slope $\left(\frac{dV}{dx} \right)_0 = w$ is proportional to the slope itself: $\sigma(w) \propto w$.

ABBM model

Introduction

One degree of freedom in a Random Energy Landscape

The ABBM model was introduced in [ABBM: Alessandro *et al.* 1990a, 1990b]. It uses a simplified description of the magnetization process in which a single DW moves in a disordered medium. The disorder is described with a random energy profile, composed by a demagnetizing term plus a stochastic pinning term. Various choices have been used for the derivative of the pinning energy, called pinning field: the brownian motion; the Ornstein–Uhlenbeck process; the Ornstein–Uhlenbeck process with an additional correlation length used to allow the reversible DW motion. Although first used to describe the Barkhausen effect, it will be introduced here for the investigation of hysteresis loops. Among the main results, we found that the hysteresis loops at low field values behave according to the Rayleigh law. We also observed that the loss separation law, observed experimentally, is a property of our model.

Definition of domain wall

By domain wall (DW) we usually mean a transition layer of a magnetized material (non saturated) where the magnetic moments rotate from the orientation in one domain to the orientation in the other. In this way the initial and final directions coincide with the direction of magnetization in the two domains that surround the domain wall. It is an interesting exercise to deduce the DW thickness when just considering the two main energies that act on its formation. The exchange energy favors thicker walls, so that the neighboring magnetic moments that form the DW have a minimum deviation angle. The anisotropy energy instead favors thinner walls, so that a minimum number of magnetic moments lies in a direction away from the easy magnetization axes.

One interesting fact about DWs, as we mentioned in the introduction, is that for a given material is sufficient to give their position and shape, together with the direction of magnetization inside the domains, to define the magnetic state of the body. That is, it is not necessary to know the direction of every magnetic moment, because at this description level we assume that inside a magnetic domain every magnetic moment points along the same direction.

Having assumed this fact, let us move a step forward, toward a simplified model: a long metallic ribbon with just one 180° DW dividing two domains, with opposite magnetization. Let us simplify further the model by neglecting any DW bowing, and supposing its thickness to be zero. We can see that in this model, the system state is just defined by the DW position, and nothing else.

The ABBM model

Dynamical and pinning field equations

We assume to have a single planar 180° DW moving across a metallic slab of thickness d and cross-section S . The only coordinate used will be its position, proportional to the magnetic flux Φ reversed during its motion. Any internal degree of freedom related to DW flexibility (bowing) is neglected, so that the DW velocity v_{DW} is the same for every point of the wall and is proportional to the magnetic flux rate of change $\dot{\Phi} = 2d \cdot I_s \cdot v_{DW}$, where I_s is the saturation magnetization of the material. Other magnetization mechanisms than DW motion, like rotations of the magnetization vector inside magnetic domains, or generation and annihilation of DWs, are not taken into account: the hysteresis properties will thus not describe the approach to saturation. The magnetization processes that will be described by our model take place in the low magnetization region around the coercive field H_c .

One degree of freedom in a Random Energy Landscape

The starting equation for the DW motion theory [Williams,Shockley,Kittel 1950] gives the DW velocity as the difference of the external field minus a counterfield H_0 :

$$\dot{\Phi} \propto H_a - H_0 \quad [7]$$

where we will assume that the counterfield be $H_0=H_{dem}+H_p$. The first term is the demagnetizing field, and a further simplification is to set it proportional to the DW displacement (that is, the magnetic flux Φ). This is a strong assumption, partly justified when observing that in a real material the demagnetizing field, originating from the free magnetic poles at the sample edges, increases as the sample increases its magnetization. A linear Φ dependence implies that the contribution to the free energy is parabolic. The second term H_p is the pinning field: the stochastic field that represents the noise encountered by the DW during its motion. An example of the resulting free energy profile and of its derivative is presented in Fig. 2 , when the DW position is indicated by the x coordinate.

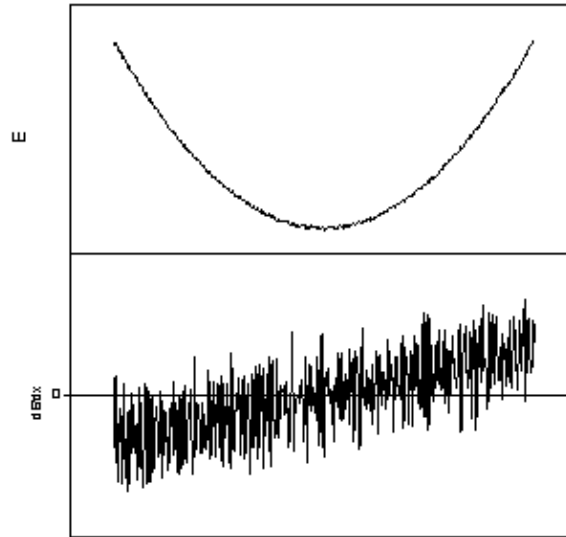


Fig. [PARABEN] Parabolic energy profile, and its derivative

Fig.2 Parabolic energy profile, and its derivative

Starting from [Eq.7] , the equality holds [ABBM]:

$$\sigma G \dot{\Phi} = H_a - \frac{\Phi}{S\mu} - H_p(\Phi) \quad [8]$$

where σ is the electric conductivity of the material, and the permeability μ characterizes the magnetostatic effects. The dimensionless coefficient G is equal to $(4 / \pi^3) \sum_{\text{odd } k} (1 / k^3) = 0.135\sigma$, when considering a wide slab ($S \gg d$). The magnetostatic field is assumed to be proportional to the flux, H

$$m = \Phi / S\mu .$$

The random pinning field was at first chosen as:

One degree of freedom in a Random Energy Landscape

$$H_p(\Phi) = W(\Phi) \quad [9]$$

that is, starting from a pure brownian (Wiener–Lèvy, WL) process $W(\Phi)$ of the variable Φ , characterized by independent increments dW , with $\langle dW \rangle = 0$ and $\langle dW^2 \rangle \propto d\Phi$. Nevertheless, this approach was considered incomplete, as the non–stationarity of the process (the linear increase of its variance) is non physical. It must in fact be observed that, as we will see in the next chapter, the variance of the pinning field is directly connected to the coercive field of the resulting hysteresis loop. It was then decided to require the stationarity of the pinning field with the aid of a correlation length, so that the pinning field was now defined as the Ornstein–Uhlenbeck process [Gardiner 1985]:

$$\frac{dH_p}{d\Phi} + \frac{H_p}{\xi_2} = \frac{dW}{d\Phi} \quad [10]$$

The pinning field H_p is obtained from $W(\Phi)$ requiring it to be stationary for large displacements $\Delta \Phi \gg \xi_2$, where ξ_2 is a correlation length, with the dimension of a magnetic flux. But another drawback was still present in this approach: being $W(\Phi)$ a fractal process, its derivative was impossible to define. Still, the derivative of the pinning field is directly connected to the reversible permeability. To be able to calculate the reversible permeability, it has been then necessary to add a second correlation length ξ_1 , such that for $\Delta \Phi \ll \xi_1$ the average pinning field slope is well defined. We then describe the random pinning field $H_p(\Phi)$ by the following set of stochastic differential equations:

$$\begin{cases} \frac{dH_p}{d\Phi} = S(\Phi) \\ \frac{dS}{d\Phi} + \left(\frac{1}{\xi_1} + \frac{1}{\xi_2}\right)S = -\frac{1}{\xi_1 \xi_2} H_p + \frac{1}{\xi_1} \frac{dW}{d\Phi} \end{cases} \quad [11]$$

We have two stochastic processes, $H_p(\Phi)$ and $S(\Phi)$, both function of the DW position. $H_p(\Phi)$ is the pinning field, while the process $S(\Phi)$ is the pinning field slope.

Here $W(\Phi)$ is the zero–mean brownian process, whose amplitude is proportional to the DW displacement:

$$\langle |dW|^2 \rangle = 2(A_H^2 / \xi_2) d\Phi \quad [12]$$

where A

H , which has the dimension of a field, measures the amplitude of H_p fluctuations.

The correlation lengths ξ_1 and ξ_2 , usually $\xi_1 < \xi_2$, are connected to $S(\Phi)$ and $H_p(\Phi)$ respectively. In fact, we can roughly define three different regions, according to the DW displacement $\Delta \Phi$ (Tab.1):

$\Delta \Phi \ll \xi_1$	H_p shows a non–null average slope ($\frac{dS}{d\Phi} \approx \frac{1}{\xi_1} \frac{dW}{d\Phi} \approx 0$; $\langle S \rangle \approx \text{const}$)
$\Delta \Phi \gg \xi_2$	H_p becomes stationary

One degree of freedom in a Random Energy Landscape

ξ_1 $\ll \Delta \Phi \ll \xi_2$	in this region $S(\Phi)$ behaves as $S \approx -\frac{H_p}{\xi_2} + \frac{dW}{d\Phi}$, so that from [Eq.11] H_p becomes the Ornstein–Uhlenbeck stationary process characterized by $\langle H_p(\Phi) \rangle \propto \exp(-\Phi / \xi_2)$ and $\langle H_p(\Phi) ^2 \rangle = A_H^2 [1 - \exp(-\Phi / \xi_2)]$.
--	---

Tab.1 Three regions for the DW displacement

The ABBM model is recovered in the limit $\xi_1 \rightarrow 0$ and $\xi_2 \rightarrow \infty$, so that for any DW displacement we will not see any reversible region, and, as long as we move along the pinning field, the DW motion will never be stationary: H

$$p(\Phi) = W(\Phi).$$

To better evaluate the properties of the set of [Eq.11], let us define some dimensionless quantities together with some useful parameters:

$$u = t / \tau \quad [13]$$

$$\tau = \sigma G S \mu$$

$$x = \Phi / \xi_2$$

$$v = \frac{dx}{du} = \tau \frac{\dot{\Phi}}{\xi_2}$$

$$h_a = \frac{H_a}{A_H}, h_p = \frac{H_p}{A_H}, w = \frac{W}{A_H}, s = \xi_2 \frac{S}{A_H}$$

The fields are normalized to the amplitude A

H of H_p fluctuations, while the flux is normalized to the correlation length ξ_2 . The coordinate x represents the (dimensionless) position of the DW, and u the (dimensionless) time, normalized by time τ which is the time scale of the eddy current decay. [Eq.8] is then rewritten as:

$$v + \left(x - \frac{h_a(u)}{\beta}\right) = -\frac{h_p(u)}{\beta}, \quad [14]$$

while [Eq.11], defining the pinning field h_p , become:

$$\begin{cases} \frac{dh_p}{dx} = s \\ \frac{ds}{dx} + \left(1 + \frac{1}{\alpha}\right)s = -\frac{h_p}{\alpha} + \frac{1}{\alpha} \frac{dw}{dx} \\ \langle dw \rangle = 0; \quad \langle |dw|^2 \rangle = 2dx \end{cases} \quad [15]$$

where we have introduced the parameters α and β :

One degree of freedom in a Random Energy Landscape

$$\alpha = \frac{\xi_1}{\xi_2}, \beta = \frac{\xi_2}{A_H S \mu} \quad [16]$$

The motion of the DW is studied by evaluating the time derivative of [Eq.14] , at constant applied field rate dh_a/du :

$$\frac{dv}{du} = \left(\frac{1}{\beta} \frac{dh_a}{du} - v \right) - \frac{1}{\beta} \frac{dh_p}{du} \quad [17]$$

Parameter description

Two parameters are essential in the preceding equations [Eq.14] and [Eq.15] . The α parameter appears only in the system of equations describing the pinning field, while the β parameter appears in the dynamic equation describing the motion of the system state along the energy landscape.

These parameters are useful to characterize the DW motion in respect to the statistical properties of the pinning field. The parameter α (with $\alpha < 1$) is the ratio between the length scale under which the reversible effects appear (ξ_1), and the scale beyond which the hp process is stationary (ξ_2). In other words, for DW displacements smaller than α , the average pinning field slope $\langle s \rangle$ is nearly constant, while, at higher displacements, it behaves approximately as a white noise, i.e. $s \approx dw/dx$. It has been introduced to partially overcome the difficulty inherent in the definition of the derivative of a fractal process. Although some definitions of this derivative has been given [Mandelbrot 1968], with the aid of the parameter α the value of $\langle s \rangle$ can be simply calculated. It is still to be discussed if this is a feature of real materials. Apparently, the reversible motion of DWs is measurable, for example in the measure of the reversible permeability of a material at a given external field. Still, no one knows for sure if this lack of hysteresis for small external field variations indicates the nonoccurrence of energy wells under a given threshold, or if the reason lies in the instrumental limits. The $\alpha \rightarrow 0$ limit indicates a completely irreversible case, as can be demonstrated taking the limit $\xi_1/\xi_2 \rightarrow 0$ in [Eq.11] : the second equation reduces itself to $S \approx -\frac{H_p}{\xi_2} + \frac{dW}{d\Phi}$, giving rise to the

Ornstein–Uhlenbeck stationary process, which is not differentiable. Another interesting case is $\alpha = 1$, in which $\xi_1 = \xi_2$; its meaning is that the process loses the memory both of the slope and of the value of the pinning field after the same displacement $x = l$.

The second parameter β is related to the demagnetizing effects: it is the ratio between the demagnetizing field $\xi_2/S\mu$ for a DW displacement of ξ_2 [Eq.16] , and the fluctuation field A

H of H_p for the same DW displacement. It should be observed that the parameter β does not appear in the pinning field definition, but just in [Eq.14] : for a pinning field $h_p(x)$, different β values change the mean slope of the function $\beta x + h_p(x)$, hence the average demagnetizing field. The role played by this parameter is to "close" the Barkhausen jumps. The average DW displacement $\langle \Delta x \rangle$ during a Barkhausen jump decreases with increasing β , as will be evident in the graphical visualization of the DW motion.

Origin of the hysteresis loop and the static limit

It is possible to directly observe the origin of the hysteresis loop, looking at the movement of the DW along the pinning field profile. In Fig.3 are shown the function $h_0 = \beta x + h_p$ and the external field h_a . Two bold arrows indicate the direction in which the state will move.

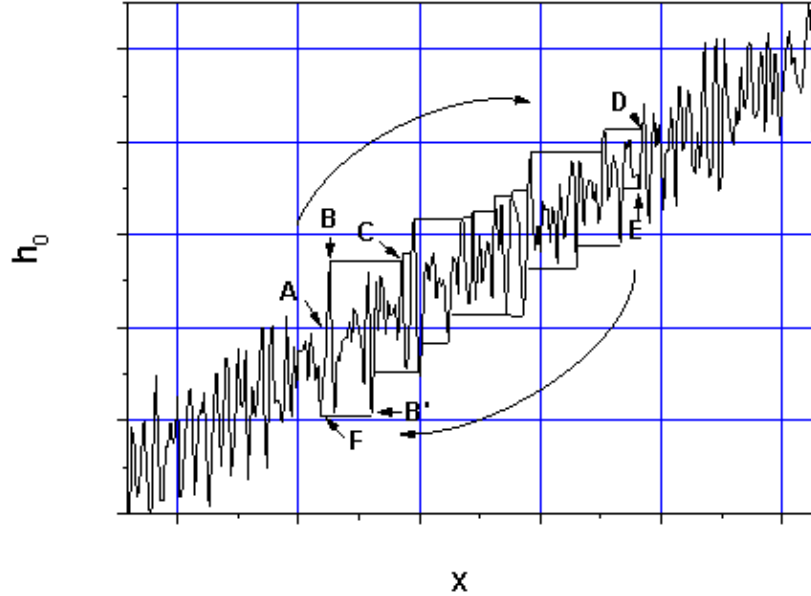


Fig.3 Birth of the hysteresis loop as a DW moves on the pinning field

We start with the DW in a stable state: at rest ($v = 0$, *stable state*), with $h_a=0$, and $h_o(x)=0$ with positive slope (point A). When increasing the applied field h_a , we observe the reversible movement of the DW (branch A–B). During the reversible motion the equality $h_a=h_0$ is valid. This motion continues until $x_{start}=h_0^{max}$ (point B), where the function h_0 presents a maximum. Here we have the irreversible jump of the DW to the next stable position (point C): the velocity from [Eq.14] is $v=(h_a-(\beta x+h_p))/\beta >0$, and the DW is in a *jump state*. The DW moves to x_{end} , such that $h_0(x_{end})=h_0^{max}$. No h_a slope is visible in the static regime, since if $dh_a/du \rightarrow 0$ the interval $x_{end}-x_{start}$ is traversed with $\Delta h_a=0$. This process continues, as the system state moves along the maxima of h_0 , until we reverse the external field direction (point D). Now, when the applied field is decreasing, the same rule is followed, but the DW jumps now at the pinning field minima (e.g., point E). From this description it should be clear the reason why the limit $\alpha \rightarrow 0$ is completely irreversible. For any Δx , an infinite number of h_0 maxima is hypothetically present, so an infinite number of Barkhausen jumps: the DW is always in a jump state.

The description given is valid in the static case, i.e. when the magnetizing frequency \dot{h}_a is nearly zero. In the next chapter we will see as this description becomes slightly modified at higher \dot{h}_a values, so that the $h_a(x)$ process is never exactly equal to $h_o(x)$, being always $h_a(x) > h_o(x)$ when h_a is increasing, and $h_a(x) < h_o(x)$ when it is decreasing. This behavior is responsible for the merging of the Barkhausen jumps in an unique sequence of continuous DW motion.

Reachable and unreachable states

Referring to Fig.3 , we see that apparently the system does not select any stable state in the interval (B–B'). We could think that this is an outcome of the magnetic hystory we have chosen, but this is not the case. We

One degree of freedom in a Random Energy Landscape

want to demonstrate that this is a general consequence of the evolution law. The result is that, given the energy landscape on which the system evolves, only a subset of the available stable states are accessible.

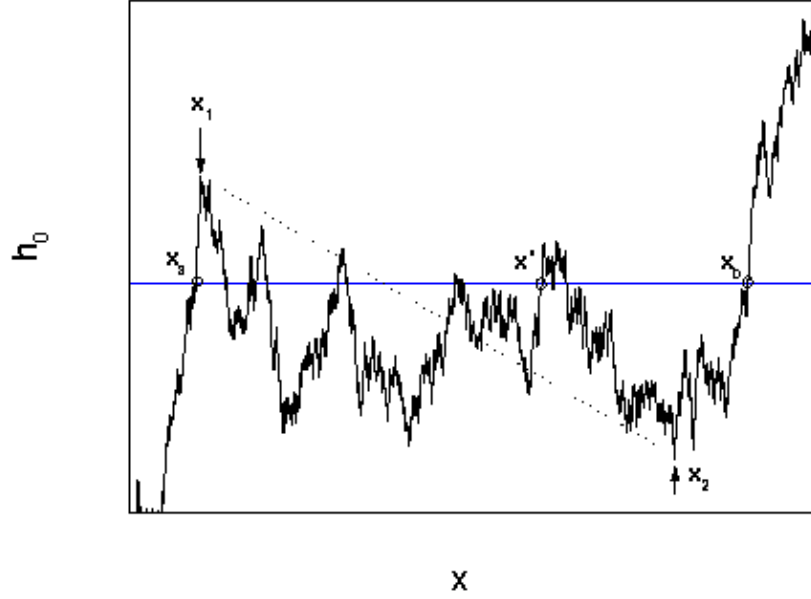


Fig.4 A set of unreachable stable states

Given a pinning field $h_p(x)$, let us consider the function $h_0(x) = \beta x + h_p(x)$, supposed continuous (see Fig.4). In the interval (x_1, x_2) let it be:

$$\left\{ \begin{array}{l} 1. h_0(x) \text{ maximum in } x_1 \\ 2. h_0(x) \text{ minimum in } x_2 \\ 3. \forall x \in (x_1, x_2) \Rightarrow h_0(x_1) > h_0(x) > h_0(x_2) \end{array} \right. \quad [18]$$

The evolution law of the states x is obtained from [Eq.14]. We already observed that the DW can either be in a *stable* state ($h_a(x) = h_0(x)$, $v = 0$) or in a *jump* state ($h_a(x) > h_0(x)$, $v > 0$). We want to demonstrate that the evolution law forbids the evolution to a stable state in the interval (x_1, x_2) .

If we start from a state $x < x_1$, evolving under an increasing field, two cases are possible:

a)

if x_1 is a stable state, then, from hypothesis 1, for $\varepsilon \rightarrow 0$, $x + \varepsilon$ will be an unstable state, and such will be any state $x > x_1$ until a state x_s where it is $h_0(x_1) = h_0(x_s)$. But this is not possible for any state in the interval (x_1, x_2) , from hypothesis 3.

b)

if x_1 is a jump state, then we search the first state $x_r < x_1$ where we have an evolution from the stable states $(x_r - \varepsilon, x_r)$ to the successive unstable states. The reasoning is then the same as in a), provided we substitute x_1 with x_r .

One degree of freedom in a Random Energy Landscape

If we start from a state $x > x_2$, evolving under a decreasing field, two cases are possible:

a)

if x_2 is a stable state, then, from hypothesis 2, for $\epsilon \rightarrow 0$, $x - \epsilon$ will be an unstable state, and such will be any state $x < x_2$ until a state x_s where it is $h_0(x_2) = h_0(x_s)$. But this is not possible for any state in the interval (x_1, x_2) , from hypothesis 3.

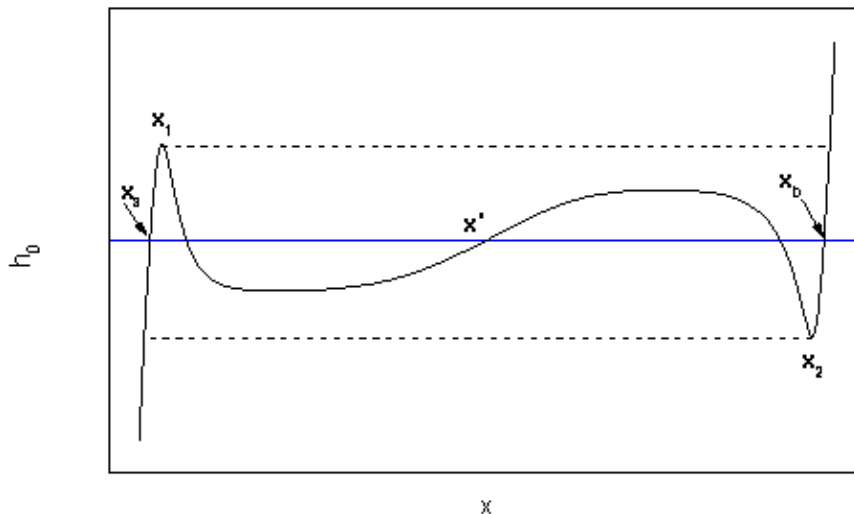
b)

if x_2 is a jump state, then we search the first state $x_r > x_2$ where we have an evolution from the stable states $(x_r + \epsilon, x_r)$ to the successive unstable states. The reasoning is then the same as in a), provided we substitute x_2 with x_r .

We thus deduce that it is impossible to arrive, with our evolution law, to any state in the interval (x_1, x_2) . What if we decided anyway to let the system start its evolution in a stable state inside this interval? Simply, the state would evolve until, when finally arriving at the state C, no field history could be able to let it come back to a stable state in (x_1, x_2) ; the evolution until this state, then, should be considered as a *transient* effect.

Great care must then be used when deciding the possible stable states where the system can be put, at the beginning of its history. How can we understand this peculiarity? At a higher abstraction level this theorem proves that we have a magnetic system where not every state is attainable with an appropriate magnetic history. This is an important conclusion when considering that a great theoretical effort has been made to understand, in various magnetic models, the nature of the demagnetized state. Considering the demagnetized state as the stable state with the lowest energy, it is an interesting question to understand if it is *possible* to reach it. We already saw in the previous chapters that the usual way to approximately reach it, both in some models and in real magnetic materials, is the AC-demagnetization, when an oscillating external field, with decreasing amplitude, slowly selects the deeper energy wells. Nevertheless, no one knows for sure if this method will exactly select the demagnetized state, because we cannot say for sure if this state is reachable.

As an example, considering again Fig.4, if the state labeled as x' was the demagnetized state, it would be impossible to reach it. Now, it is possible to show that this can happen: the demagnetized state of the system *can* be unreachable.



One degree of freedom in a Random Energy Landscape

Fig.5 The demagnetized state can be unreachable

Referring now to Fig.5 , we can see that we have three stable states: x_a , x' , x_b ; the state x' is not reachable due to the couple of extrema x_1 , x_2 , as we already demonstrated. If x' is the demagnetized state then, obviously:

$$E(x') < E(x) \quad \forall x \quad [19]$$

Its energy $E(x')$ can be calculated from the integration of the field $h_0(x)=\beta x+ h_p(x)$ which we know to be the derivative of the free energy. We can write:

$$E(x') = E(x_2) + \int_{x_a}^{x'} h_0(x) \quad [20]$$

and:

$$E(x') = E(x_b) - \int_{x'}^{x_b} h_0(x) \quad [21]$$

but, from [Eq.19] it follows:

$$\begin{cases} \int_{x_a}^{x'} h_0(x) < 0 \\ \int_{x'}^{x_b} h_0(x) > 0 \end{cases} \quad [22]$$

Now from Fig.5 we see that this condition is satisfied: it follows then that the demagnetized state, at least in an *ad hoc* built pinning field, can be unreachable.

Analytical results

Some interesting results about the energetic and hysteretic aspects of our problem can be obtained when investigating the statistical properties of the pinning field. While for a brownian type pinning field [Eq.9] or for the Ornstein–Uhlenbeck process this problem has been completely worked out, for more complex processes this is not the case. To obtain some insight in the stochastic process [Eq.15] we calculated the joint probability distribution $P(s, hp)$ of the pinning field hp and of the slope s .

Solution of the Fokker–Planck equation

The set of stochastic equations [Eq.15] defines a markovian stationary process, whose solution in close analytic form raises some mathematical difficulties. A useful analytical solution is the joint probability distribution $P(s, hp)$ of the pinning field hp and of s , as it can be calculated by the Fokker–Planck equation [Gardiner 1985, Van Kampen 1981, Papoulis 1991] associated to [Eq.15] :

$$\frac{\partial P}{\partial x} = \frac{\partial}{\partial s} \left(\frac{1}{\alpha} h_y P \right) - \frac{\partial}{\partial s} \left(- \left(1 + \frac{1}{\alpha} \right) s P \right) - \frac{\partial}{\partial h_y} (s P) + \frac{\partial^2}{\partial s^2} \left(\frac{1}{\alpha^2} P \right) \quad [23]$$

Its exact solution is:

$$P(Y, x) = \frac{1}{2\pi \sqrt{\text{Det} \Xi}} \exp \left[-\frac{1}{2} (\bar{Y} - \langle \bar{Y} \rangle) \Xi^{-1} (Y - \langle Y \rangle) \right] \quad [24]$$

where the Y vector is:

$$Y = \begin{pmatrix} h_y \\ s \end{pmatrix} \quad [25]$$

and:

$$\Xi = \begin{pmatrix} \langle s^2 \rangle - \langle s \rangle^2 & -\langle h_y s \rangle + \langle h_y \rangle \langle s \rangle \\ -\langle h_y s \rangle + \langle h_y \rangle \langle s \rangle & \langle h_y^2 \rangle - \langle h_y \rangle^2 \end{pmatrix} \quad [26]$$

The variances are the following:

$$\sigma_{h_y}^2 = \frac{1}{\alpha + 1} - \frac{1}{(\alpha - 1)^2} e^{-2x} - \frac{\alpha}{(\alpha - 1)^2} e^{-2x/\alpha} + \frac{4\alpha}{(\alpha - 1)^2 (\alpha + 1)} e^{-(1+1/\alpha)x} \quad [27]$$

$$\sigma_s^2 = \frac{1}{\alpha(\alpha + 1)} - \frac{1}{(\alpha - 1)^2} e^{-2x} - \frac{1}{\alpha(\alpha - 1)^2} e^{-2x/\alpha} + \frac{4}{(\alpha - 1)^2 (\alpha + 1)} e^{-(1+1/\alpha)x} \quad [28]$$

Apart from the constant terms $1/(\alpha + 1)$ and $1/(\alpha(\alpha + 1))$, three exponentially decaying terms are present in the variances, that represent the transient effects. After starting from any stable state, the pinning field and slope variances will be seen changing until developing a constant value, as expected from the stationary character of the process at large displacements.

Stationary solution of the Fokker–Planck equation

The equation [Eq.24] assumes a simpler form in the stationary limit. We can then calculate it in the $x \rightarrow \infty$ limit, obtaining:

$$P(s, h_y) = \frac{\sqrt{\alpha(\alpha + 1)}}{2\pi} e^{-\frac{\alpha+1}{2} h_y^2} e^{-\frac{\alpha(\alpha+1)}{2} s^2} \quad [29]$$

One degree of freedom in a Random Energy Landscape

from which the stationary amplitude distributions for the pinning field slope s and for the pinning field h

p , are:

$$P(s) = \sqrt{\frac{\alpha(\alpha+1)}{2\pi}} \exp(-\alpha(\alpha+1)s^2/2) \quad [30]$$

$$P(h_p) = \sqrt{\frac{\alpha+1}{2\pi}} \exp(-(\alpha+1)h_p^2/2) \quad [31]$$

These are gaussian distributions of zero mean and variance:

$$\sigma_s^2 = 1/(\alpha(\alpha+1)) \quad [32]$$

$$\sigma_{h_p}^2 = 1/(\alpha+1) \quad [33]$$

It's interesting to note that the widths of the distributions are uniquely determined from the parameter α . As we said, Kronmüller [Kronmüller *et al.* 1992] similarly obtained gaussian distributions for the same quantities.

The Rayleigh loop

It has been demonstrated back in the XIX century that the hysteretic properties of a ferromagnetic materials, after demagnetization, are described at low fields by the Rayleigh law:

$$I = aH + bH^2 \quad [34]$$

and the hysteresis loops sharing this shape are known as Rayleigh loops. This law is very general in its form, as the a and b parameters are not defined. One of its consequences is the cubic dependence of the loss (hysteresis loop area) with the applied field:

$$W = \frac{4}{3}bH^3 \quad [35]$$

dependence that can be simply obtained from the integration of [Eq.34].

Various theoretical efforts have been devoted to the explanation of the Rayleigh law: they are summarized in [Néel 1942, Néel 1943]. Among them, it must be remarked the work of Weiss and Freudenreich, which explained [Eq.34] using a model which, many years later, became known as the Preisach model (see below). As will be shown here, in the model we developed the Rayleigh law is an implicit feature, as it comes out of the statistic of the pinning field. We will try in the following to show the relationships of the a and b parameters to the predictions obtained from Néel's work and from the Preisach model.

Néel's model

One degree of freedom in a Random Energy Landscape

Néel's model has been used in our simulations to test the correctness of our approach. We already discussed the basics of the model he developed, and the pinning field profile he used in its calculations. Having to investigate the response of the system at the demagnetized state, that is the state lying in the deeper energy well, Néel classified the possible configurations that an energy well can feature, calculating the probabilities for the DW to be in each one of them. From this calculation he was able to obtain the Rayleigh law, in the form

$$I = 0.81 \cdot H + \frac{1}{\pi} H^2 \quad [36]$$

so that the parameters have the values $a=0.81$ and $b=1/\pi$. He then applied this result to the study of materials divided in many magnetic domains, being able to obtain the coercive field value for loops at high fields.

-

Preisach model and the irreversible parameter

b

In the Preisach model the DW motion is not considered at all. Instead, the hysteresis loops are obtained from the superposition of single square loops (*hysterons*) of different width h_c , and different displacement h_u relative to the $H=0$ axis. The hysteretic behavior is characterized by a function, the Preisach distribution $P(h_c, h_u)$, which gives the relative weight of each hysteron in the superposition. In [Bertotti, Basso, Magni 1998] it is shown that the ABBM model is equivalent to the Preisach model, with an appropriate distribution $P(h_c, h_u)$ [Eq.37]. Unfortunately, this equivalence has not been demonstrated for the more complex case [Eq.11], but just for the Wiener–Lévy process [Eq.9].

Mayergoyz [Mayergoyz 1991] demonstrated that two properties, known as the wiping-out property and the congruency property, represent necessary and sufficient conditions under which a system can be described by the Preisach model. Consider that, under the applied field history (h_0, h_1, h_2, h_1) , with the restriction $h_0 < h_1 < h_2$, the system state is correspondingly described by the sequence $\{S_a, S_b, S_c, S_d\}$. The wiping-out rule states that the system states S_a and S_d are exactly the same. Let us recall that in our model the system state is defined by the variable x only. The congruency rule states that all minor loops, delimited by the same peak field values are geometrically congruent. Bertotti *et al.* demonstrated, using this model, that the wiping out rule is satisfied, while the congruency rule is followed by the average loops only. So we can be confident that the average hysteresis loops obtained with our model can even be obtained with the right choice of Preisach distribution. This distribution is of the type

$$p(H_c) = 2g \frac{gH_c \coth(gH_c) - 1}{\sinh^2(gH_c)} \quad [37]$$

where $g = \beta \xi_2 / A_H^2$. We will observe that this distribution in the Preisach plane does depend on the coercive field only, and not on the interaction field H_u . This is due to the non saturation of the hysteresis loops obtained in our model. The integration of this distribution using the normalized variables gives the relation between the DW displacement and the applied field, which results, at small hm , $x_m \approx h_m^2 / 3$,

$$x_m = \frac{h_m^2}{3} \quad [38]$$

One degree of freedom in a Random Energy Landscape

i.e. $a = 0$ and $b = 1/3$. We will see that this result fits well with our data for low values of the reversible parameter. This conclusion is very important, as it confirms the equivalence of our model with the Preisach model, in the $\alpha \rightarrow 0$ limit.

We can extend this result trying to calculate the first order dependence in α of the b parameter. To obtain an approximate expression for $b(\alpha)$ we can write the approximate form of [Eq.15] at low α values, and $h_p \approx 0$:

$$\begin{cases} \frac{dh_p}{dx} = s \\ (1+\alpha)s = \frac{dw}{dx} \end{cases} \quad [39]$$

from which, following the same reasoning that lead to [Eq.38], one obtains:

$$b = \frac{1}{3}(1+\alpha)^2 \quad [40]$$

ABBM model

The ABBM model can be used to foresee the values of the a Rayleigh parameter. It has been shown in a similar model [Pfeffer 1967] that this calculation can be performed once it is known the occupation probability of the low energy states $g(s)$ as a function of the pinning field slope s . The reason is that the Rayleigh loops are obtained starting from the lowest energy state for each pinning field instance. The a parameter is related to the inverse of the pinning field slope, so we will calculate the average value of the inverse of the slope s :

$$\alpha = \frac{\int_0^{\infty} ds P(s) \frac{g(s)}{s}}{\int_0^{\infty} ds \frac{P(s)}{s}} \quad [41]$$

once we impose a dependence of the kind $g(s)=s\eta$, we obtain:

$$\alpha = \sqrt{\frac{\alpha(\alpha+1)}{2}} \frac{\Gamma\left(\frac{\eta}{2}\right)}{\Gamma\left(\frac{\eta+1}{2}\right)} \quad [42]$$

The comparison of theoretical and simulation results (Tab.3) shows, as we will see later, that there is an adequate agreement with the a value found from the permeability simulations when imposing $\eta = \alpha + 1$:

$$\left\{ \begin{array}{l} g(s) = s^{\alpha+1} \\ \alpha = \sqrt{\frac{\alpha(\alpha+1)}{2}} \frac{\Gamma\left(\frac{\alpha+1}{2}\right)}{\Gamma\left(\frac{\alpha+2}{2}\right)} \end{array} \right. \quad [43]$$

Hysteresis loop simulations: the numerical integration

A general solution is calculated by numerically integrating [Eq.17] . The first step was to use as pinning field a random polygonal line generated according to Néel's prescriptions. As we said, in this way we have been able to test our procedure, because the Rayleigh parameters are analytically known for this pinning field. Néel's pinning field was obtained for our simulations by generating a random polygonal line with $2l=1$ and a slope following a gaussian distribution with width $P_0=1$, [Eq.4] . Being satisfied with the results obtained, we changed the pinning field using the one defined in [Eq.15] . The generation of the ensemble of pinning field profiles $hp(x)$ was accomplished through the integration of [Eq.15] over discrete steps Δx and for different $w(x)$ processes. We are talking here about an *ensemble* of pinning fields because reasonable results are only obtained when averaging many times the hysteresis loops obtained. To correctly discretize the fine structure of $hp(x)$, the minimum step Δx used in the generation of the field is chosen to be $\Delta x \ll \alpha$ (typically $\Delta x = 10-2\alpha$): that is, the DW moves 100 steps through the reversible region, for any α value. For each profile, the DW velocity $v(u)$ is calculated by [Eq.17] over discrete time steps Δu , in the case of triangular external field $ha(u)$ of amplitude hm . We want to stress here what we already mentioned in the preceeding paragraph (*Origin of the hysteresis loop and the static limit*): the simulations we are talking about here are *static*, that is the external field variation during time is $\dot{h}_a(u) \rightarrow 0$. This procedure will ensure that the shape of the loops investigated will origin from the underlying pinning field statistics only, and will not be modified by dynamical effects, whose influence on the loop shape will be studied in the next chapter.

The initial condition is that of a DW positioned at the energy minimum of the generated pinning field, so that our and Néel's results will be comparable. To avoid spurious effects due to transients, no data is recorded from the simulations until a fixed number of loops along the pinning field has been performed.

The whole procedure here described is repeated for every pinning field in the ensemble, and the loops are finally averaged. In principle, the calculation of hysteresis loops can be performed using two different procedures. Using [Eq.15] , the pinning field can be generated at each time step to directly calculate the increment of the DW velocity; or it can be generated *ab initio* as a spatial quenched-in profile, and kept fixed along an entire hysteresis loop. In this case, the two half loops are correlated in a specular way, and this result, although possible in principle, has not been physically observed until now. On the other hand, when the hysteresis loop properties are averaged over a statistical ensemble of pinning fields, there is really no difference between the two methods.

-

Simulations

Static loops: the parameters' choice

The set of parameters $\{\alpha, \beta\}$, together with the maximum field amplitude h_m , allows us to explore a wide range of hysteretic phenomena.

One degree of freedom in a Random Energy Landscape

The parameter α sets the reversible effects length scale: for DW displacements smaller than α , the average pinning field slope $\langle s \rangle$ is nearly constant, while for higher values the jerky h_p behavior becomes visible.

The parameter β changes the demagnetizing effects: at high DW displacements x_m , we have from [Eq.14] : $x_m \sim h_m/\beta$: a proportionality between the maximum external field applied and the maximum DW displacement. This means that we are in presence of a so-called *magnetostatic* hysteresis loop, whose average slope $1/\beta$ is clearly visible. We are now, indeed, outside the Rayleigh region where the loop shape is not rectangular but, as we said, parabolical.

As already stated, we are not able to extend our model to include the effects – rotations, DW nucleation, annihilation – appearing towards saturation. So we focused on the Rayleigh region, where we expected to find the Rayleigh law:

$$x_m = a h_m + b h_m^2 \quad [44]$$

where h_m is the peak applied field, and x_m is the amplitude of the average hysteresis loop. We studied also the way the parabolic hysteresis loops modify themselves when entering into the region dominated from the magnetostatic fields, where the hysteresis loop permeability attains a constant value. Hysteresis loops are calculated in the case of low demagnetizing field, that is $\beta = 0.1$. Here, low means a low ratio of the demagnetizing field to pinning field fluctuation amplitude. This choice will be justified in the following, where we will see as the parameter β allows to change the extension of the Rayleigh and magnetostatic regions in the x_m/h_m vs. h_m plane.

The regime chosen in the first set of simulations is static, and different influences of reversible effects were chosen:

1)	$\alpha = 0$	no reversible effects (Ornstein–Uhlenbeck process, [Eq.10])
2)	$\alpha = 0.01$	negligible reversible effects
3)	$\alpha = 0.5$	a case directly comparable to the Néel's result (see below)
4)	$\alpha = 1$	where the two correlation lengths ξ_1 and ξ_2 are equal

Tab.2 Parameter α choices

In our first simulations, however, the pinning field was not obtained with the integration of [Eq.15], but following Néel's description, that is from the derivative of a sequence of parabolic arcs with the same spacing $2l$ along the x axis, corresponding in our case to the distance ξ_2 . This check allowed us to be confident on the precision of the simulations.

Simulation results

There are two possible ways we can obtain the Rayleigh parameters from our simulations. We can study the permeability x_m/h_m as a function of the applied field h_m (Fig.7): in this way we will obtain the a value from the intercept at $h_m=0$, while the slope at this point will give the b value. Another possible way is to integrate the Rayleigh law, obtaining in this way the static loss W_0 :

One degree of freedom in a Random Energy Landscape

W_0

$$= (4/3)bhm^3 \quad [45]$$

We can then use the function $(3/4)W_0/h_m^3$ (Fig.8) as an alternative estimate of the b value vs. the applied field h_m .

The first result to mention is that the Rayleigh law [Eq.44] was always found valid, at least at low peak fields h_m where the demagnetizing fields still do not modify the loop shape, Fig.6 . When we talk about low fields we mean, as we discussed before, that we are in the region (region (A) of Fig.7), where the maximum DW displacement is such that $0 < x_m < 1$. In this region the hysteresis loops are neatly described with the parabolic law [Eq.44].

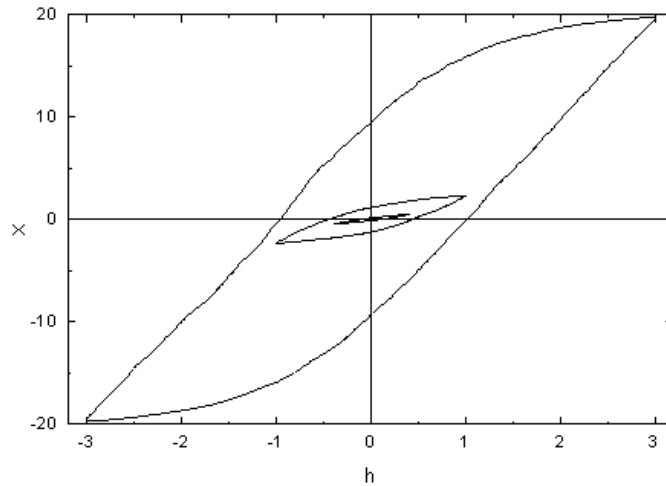


Fig.6 Three hysteresis loops of different amplitudes, showing the behavior in the Rayleigh region (inner loops) and of the demagnetizing field (outer loop)

Fig.7 gives a summary of the hysteresis loop behaviors, showing the ratio x_m/h_m as a function of the applied field h_m .

One degree of freedom in a Random Energy Landscape

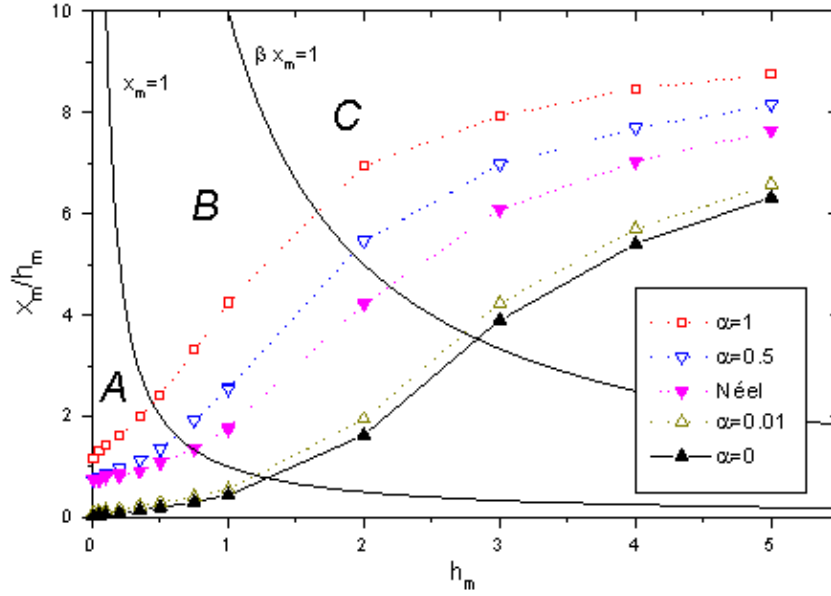


Fig.7 The permeability ratio for different pinning fields. The *Néel* label indicates simulations performed using Néel's prescription for the pinning field.

An important result is that three distinct regions can be clearly recognized. The first one is the Rayleigh region (A) at low applied fields. The property of this region is that the permeability is linear, and the hysteresis loops have a clearly defined parabolic shape. An example of these kind of loops is visible looking at the inner loops in Fig.6 , following the Rayleigh relationship [Eq.44]. This occurs up to x

$m \sim 1$, i.e. up to DW displacements ϕm of the order of the correlation length ξ^2 . This means that we are exploring a region where the pinning field is not yet stationary, so its fluctuations are growing as the square root of the DW displacement. And this the possible explanation of the Rayleigh law: we believe that the quadratic form of this law be connected to the fact that the stochastic process that lies at the basis of the system of equations [Eq.15] is the brownian motion process $w(x)$. Due to the fact that its variance increases with the distance as $\langle |dw|^2 \rangle \propto dx$, we obtain the relationship $\Delta x \propto \Delta h^2$ between the field variation and the DW displacement. A stochastic process of the fractional brownian motion type $f(x)$, that exhibits a variance $\langle |df|^2 \rangle \propto dx^{2H}$, with $0 < H < 1$ the Hurst exponent, would show a Rayleigh law of the $\Delta x \propto \Delta h^{1/H}$ form. In the case of the brownian motion, $H=1/2$ and the Rayleigh law holds.

In the intermediate region (B), the DW moves in a stationary pinning field (ϕ

$m \gg \xi^2$), but the demagnetizing effects are still negligible: the latter become dominating when the demagnetizing field $\phi m / S\mu$ overcomes the pinning field fluctuation amplitude AH , so when $\beta x m \sim 1$. The role of this region is that of linking the Rayleigh region (A) to the magnetostatic region (C). Being then influenced from both regions, a simple modeling of the loops here is not easy. Last, there is a high field region (C) fully dominated by the magnetostatic effects, where the permeability tends to saturate to the $1/\beta$ value, as the applied field approaches the amplitude of the magnetostatic field, $h_a \sim h_m \sim \beta x_m$. The trend towards the $1/\beta$ value is more slow for low α values, because the starting slope (b value) in their case is lower. The hysteresis loops exhibit here a rectangular shape, their width being given from the value of σ_{k_0} .

Obviously, the extension of the intermediate region (B) strongly depends on the value of the parameter β as it is delimited by the curves x

One degree of freedom in a Random Energy Landscape

$m \sim 1$ and $\beta x m \sim 1$, and disappears as β approaches 1 . So a value of β too high would shrink the (B) region, eventually destroying it. Physically, this means that the magnetostatic effects in this case are so strong to appear in the Rayleigh region, and the Rayleigh loops lose their parabolic shape. For our choice of β the shape of the loops in the three regions is shown in Fig.6 .

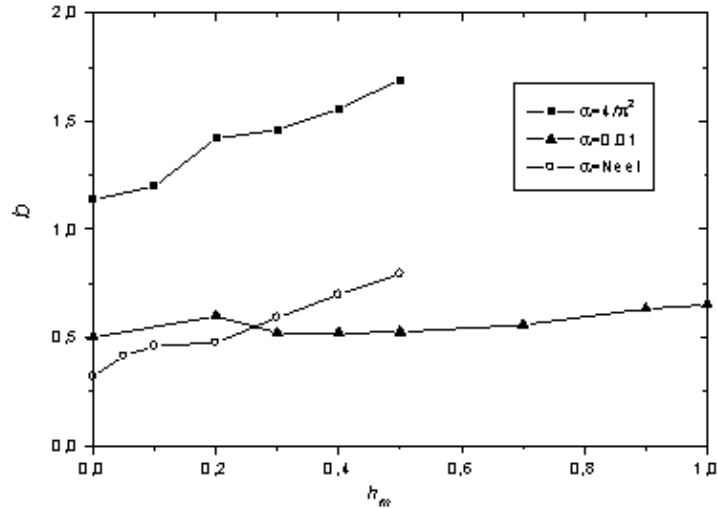


Fig.8 The parameter b value from the loss at low fields

We use $(3/4)W_0/h_m^3$ (Fig.8) as an alternative estimate of the b value vs. the applied field h_m . Here we report two α values, respectively $\alpha = 0.5$ and $\alpha = 0.01$. Néel's result calculated through numerical simulations using a saw-tooth pinning field is also reported. The correct b value must be searched in the $h_m \rightarrow 0$ limit (Rayleigh region). It is possible to observe that its value in the $\alpha = 0.01$ case remains almost constant, contrary to the other two cases: this is due to the fact (Fig.7) that in this case the Rayleigh region (A) is much more extended as a function of h_m .

Models comparisons

In Tab.3 we summarized from one side the results obtained with our simulations, while on the other side are shown the analytical results that we've been able to obtain from the ABBM model (for the value of a) and from the Preisach model (for the value of b). A last analytical result is the already mentioned solution for Néel's model, in which $a = 0.81$ and $b = 1/\pi \approx 0.3183$.

	Computer Simulations			Analytical Results	
	Permeability		Losses	[Eq.43]	[Eq.40]
	a	b	b	a	b
$\alpha = 1$	1.17	2.34	—	1.13	1.33

One degree of freedom in a Random Energy Landscape

$\alpha = 0.5$	0.73	1.18	1.20	0.83	0.75
Néel	0.74	0.49	–	–	–
$\alpha = 0.01$	0.09	0.41	0.52	0.13	0.34
$\alpha = 0$	0.02	0.34	–	0	0.33

Tab.3 Rayleigh parameters estimates from computer simulations and from analytical results.

Néel's pinning field was obtained for our simulations by generating a random polygonal line with $2l=1$ and a slope following a gaussian distribution with width $P_0=1$. In our simulations, when using this pinning field, we find values for the a and b parameters comparable with Néel's results (ex. in Fig.8 we can see that the limit value for b is $b \approx 1/\pi$, as calculated by Néel).

The case $\alpha = 0.5$ has been chosen being the case that reported the result for a closest to Néel's model. We found in fact $a=0.73$. Néel's result for the parameter $b \approx 1/\pi$ is instead far from our result $b \approx 1.20$, but the difference in the much higher b value can be explained. It should be stressed in fact that our pinning field is not exactly the same as a random polygonal line. In the ABBM case small fluctuations are always admitted, depending on the step resolution chosen for generating the pinning field stochastic function. For steps $\Delta x < \xi$, Néel's pinning field is exactly a straight line, while in our case small fluctuations are still present, although the motion is largely reversible. This effect is visible when using the pinning field defined according to Néel's description, as we saw: in this case the b value obtained drops to $b \approx 0.35$. Moreover, the results for Néel's model were obtained from a calculation assuming the DW started from the demagnetized state, while in our case the DW starts from a random stable position. Just a fixed number of stabilization loops have been performed in our simulations, to eliminate any transient effects. Both the reasons showed should contribute to a greater loss value, and therefore a greater b value.

A comparison between the a values and [Eq.43], which is the prediction obtained for the reversible parameter, shows that the population distribution at the low energy states is $g(s) = s\alpha^{-1}$, and imposing this behavior the calculated a parameter fits well the data. The law we found differs slightly from the analogous law that is found in [Pfeffer 1967, Kronmuller *et al.* 1992, Hilzinger *et al.* 1976, Reininger *et al.* 1992]. In that model, the distribution was linearly dependent on the pinning field slope. In our case, the linear behavior is valid just at $\alpha = 0$, while higher α values give in return steeper dependences of the distribution on the pinning field slope.

The equation [Eq.40] obtained from the equivalence between the ABBM model – in the Wiener–Lévy case – and the Preisach model, underestimates the b value at high α values, while obtaining good results when α is low. This result is not surprising, since the approximation is valid at first order in α .